Well-balanced finite volume evolution Galerkin methods for the shallow water equations

M. Lukáčová - Medviďová[1], S. Noelle[2] and M. Kraft[1]

Abstract

We present a new well-balanced finite volume method within the framework of the finite volume evolution Galerkin (FVEG) schemes. The methodology will be illustrated for the shallow water equations with source terms modelling the bottom topography and Coriolis forces. Results can be generalized to more complex systems of balance laws. The FVEG methods couple a finite volume formulation with approximate evolution operators. The latter are constructed using the bicharacteristics of the multidimensional hyperbolic systems, such that all of the infinitely many directions of wave propagation are taken into account explicitly. We derive a well-balanced approximation of the integral equations and prove that the FVEG scheme is well-balanced for the stationary steady states as well as for the steady jets in the rotational frame. Several numerical experiments for stationary and quasi-stationary states as well as for steady jets confirm the reliability of the well-balanced FVEG scheme.

Key words: well-balanced schemes, steady states, systems of hyperbolic balance laws, shallow water equations, geostrophic flow, evolution Galerkin schemes

AMS Subject Classification: 65L05, 65M06, 35L45, 35L65, 65M25, 65M15

1 Introduction

Consider the balance law in two space dimensions

$$\boldsymbol{u}_t + \boldsymbol{f}_1(\boldsymbol{u})_x + \boldsymbol{f}_2(\boldsymbol{u})_y = \boldsymbol{b}(\boldsymbol{u}, x, y), \tag{1.1}$$

where $\boldsymbol{u}$ is the vector of conservative variables, $\boldsymbol{f}_1$, $\boldsymbol{f}_2$ are flux functions and $\boldsymbol{b}(\boldsymbol{u}, x, y)$ is a source term. In this paper we are concerned with the finite volume evolution Galerkin (FVEG) method of Lukáčová, Morton and Warnecke, cf. [18]-[23]. The FVEG methods couple a finite volume formulation with approximate evolution operators which are based on the theory of bicharacteristics for the first order systems [18]. As a result exact integral equations for linear or linearized hyperbolic conservation laws can be derived, which take into account all of the infinitely many directions of wave propagation. In the finite volume

[1]Department of Mathematics, University of Technology Hamburg, Schwarzenbergstraße 95, 21 079 Hamburg, Germany, emails: lukacova@tu-harburg.de, kraft@tu-harburg.de

[2]Division of Numerical Mathematics IGPM, RWTH Aachen, Templergraben 55, 52062 Aachen, Germany, email: noelle@igpm.rwth-aachen.de

framework the approximate evolution operators are used to evolve the solution along the cell interfaces up to an intermediate time level $t_{n+1/2}$ in order to compute fluxes. This step can be considered as a predictor step. In the corrector step the finite volume update is done. The FVEG schemes have been studied theoretically as well as experimentally with respect to their stability and accuracy. Extensive numerical experiments confirm robustness, good multidimensional behaviour, high accuracy, stability, and efficiency of the FVEG schemes, see, e.g. [21], [22]. We refer the reader to [1], [6], [7], [8], [15], [25] for other recent multidimensional schemes.

For balance laws with source terms, the simplest approach is to use the operator splitting method which alternates between the homogeneous conservation laws

$$\boldsymbol{u}_t + \boldsymbol{f}_1(\boldsymbol{u})_x + \boldsymbol{f}_2(\boldsymbol{u})_y = 0$$

and the ordinary differential equation

$$\boldsymbol{u}_t = \boldsymbol{b}(\boldsymbol{u}, x, y)$$

at each time step. For many situations this would be effective and successful. However, the original problem (1.1) has an interesting structure, which is due to the interplay between the differential terms and the right-hand-side source term during the time evolution. For many flows which are of interest in geophysics, the terms are nearly perfect balanced. If these terms are treated separately in a numerical algorithm, the fundamental balance may be destroyed, resulting in spurious oscillations. In particular, we will be interested to approximate correctly equilibrium states or steady states, i.e. such $\boldsymbol{u}$ that

$$\boldsymbol{f}_1(\boldsymbol{u})_x + \boldsymbol{f}_2(\boldsymbol{u})_y = \boldsymbol{b}(\boldsymbol{u}, x, y).$$

These equilibrium solutions play an important role because they are obtained usually as a limit when time tends to infinity.

In this paper we present an approach which allows to incorporate treatment of the source in the framework of the FVEG schemes without using the operator splitting approach. As a result the steady states, or quasi-steady states, will be approximated correctly. The scheme is called the *well-balanced finite volume evolution Galerkin scheme*, see also [2], [4], [5], [9],[11], [14], [16], [26], [27] for other related approaches for finite volume and finite difference schemes.

Our paper is organized as follows. In Section 2 a brief description of the finite volume evolution Galerkin scheme is given. Applying the theory of bicharacteristics for multidimensional first order systems of hyperbolic type the exact evolution operator is derived. A well-balanced approximation of the exact evolution operator, which preserves some interesting steady states exactly and also works well for their perturbations, will be constructed in Section 3. In Section 4 we summarize the main steps of the FVEG method and present its algorithm. Further, we prove that the FVEG scheme is well-balanced for the stationary steady states (e.g. lake at rest) as well as for the steady jets on the rotating plane. Numerical experiments for one and two-dimensional stationary and quasi-stationary problems as well as for steady jets presented in Section 5 confirm reliability of the well-balanced FVEG scheme. The question of positivity preserving property of the scheme, i.e. $h > 0$, is not yet considered here and will be addressed in our future paper.

2 Finite volume evolution Galerkin schemes

There are many practical applications where the balance laws and the correct approximation of their quasi-steady states are necessary. Some example include shallow water equations with the source term modelling the bottom topography, which arise in oceanography and atmospheric science, gas dynamic equations with geometrical source terms, e.g. a duct with variable cross-section, or fluid dynamics with gravitational terms. In what follows we illustrate the methodology on the example of the shallow water equations with the source terms modelling the bottom topography and the Coriolis forces. This system reads

$$\boldsymbol{u}_t + \boldsymbol{f}_1(\boldsymbol{u})_x + \boldsymbol{f}_2(\boldsymbol{u})_y = \boldsymbol{b}(\boldsymbol{u}), \tag{2.1}$$

where

$$\begin{aligned} \boldsymbol{u} &= \begin{pmatrix} h \\ hu \\ hv \end{pmatrix}, \ \boldsymbol{f}_1(\boldsymbol{u}) = \begin{pmatrix} hu \\ hu^2 + \frac{1}{2}gh^2 \\ huv \end{pmatrix}, \\ \boldsymbol{f}_2(\boldsymbol{u}) &= \begin{pmatrix} hv \\ huv \\ hv^2 + \frac{1}{2}gh^2 \end{pmatrix}, \ \boldsymbol{b}(\boldsymbol{u}) = \begin{pmatrix} 0 \\ -ghb_x + fhv \\ -ghb_y - fhu \end{pmatrix}. \end{aligned}$$

Here h denotes the water depth, u, v are vertically averaged velocity components in $x-$ and $y-$ direction, g stands for the gravitational constant, f is the Coriolis parameter, and $b = b(x, y)$ denotes the bottom topography. Note that these equations are also used in climate modelling and meteorology for geostrophic flow, see, e.g., [4], [12]. For simulation of river or oceanographic flows some additional terms modelling the bottom friction need to be considered as well.

Let us divide a computational domain Ω into a finite number of regular finite volumes $\Omega_{ij} = [x_{i-\frac{1}{2}}, x_{i+\frac{1}{2}}] \times [y_{j-\frac{1}{2}}, y_{j+\frac{1}{2}}] = [x_i - \hbar/2, x_i + \hbar/2] \times [y_j - \hbar/2, y_j + \hbar/2]$, $i, j \in \mathbb{Z}$, $\hbar$ is a mesh step. Denote by $\boldsymbol{U}_{ij}^n$ the piecewise constant approximate solution on a mesh cell Ω_{ij} at time t_n and start with initial approximations obtained by the integral averages $\boldsymbol{U}_{ij}^0 = \int_{\Omega_{ij}} \boldsymbol{U}(\cdot, 0)$. Integrating the balance law (2.1) and applying the Gauss theorem on any mesh cell Ω_{ij} yields the following finite volume update formula

$$\boldsymbol{U}_{ij}^{n+1} = \boldsymbol{U}_{ij}^n - \lambda \sum_{k=1}^{2} \delta_{x_k}^{ij} \bar{\boldsymbol{f}}_k^{n+1/2} + \Delta t \boldsymbol{B}_{ij}^{n+1/2}, \tag{2.2}$$

where $\lambda = \Delta t/\hbar$, Δt is a time step, $\delta_{x_k}^{ij}$ stays for the central difference operator in the x_k-direction, $k = 1, 2$ and $\bar{\boldsymbol{f}}_k^{n+1/2}$ represents an approximation to the edge flux at the intermediate time level $t_n + \Delta t/2$. Further $\boldsymbol{B}_{ij}^{n+1/2}$ stands for the approximation of the source term $\boldsymbol{b}$. The cell interface fluxes $\bar{\boldsymbol{f}}_k^{n+1/2}$ are evolved using an approximate evolution operator denoted by $E_{\Delta t/2}$ to $t_n + \Delta t/2$ and averaged along the cell interface edge denoted by $\mathcal{E}$. The well-balanced approximate evolution operators will be derived for the shallow water equations in the next section.
For the first order scheme the approximate evolution operator $E_{\Delta t/2}^{const}$ for the piecewise constant data is used, cf. Section 3, and the fluxes are evaluated as follows

$$\bar{\boldsymbol{f}}_k^{n+1/2} := \frac{1}{\hbar} \int_{\mathcal{E}} \boldsymbol{f}_k(E_{\Delta t/2}^{const} \boldsymbol{U}^n) \mathrm{d}S. \tag{2.3}$$

For the second order method the continuous bilinear recovery R_h is applied first. Then the predicted solution at cell interfaces is obtained by a suitable combination of E_Δ^{const} and E_Δ^{bilin}. We use E_Δ^{bilin} to evolve slopes and E_Δ^{const} to evolve the corresponding constant part in order to preserve conservativity

$$\bar{\boldsymbol{f}}_k^{n+1/2} := \frac{1}{\hbar}\int_{\mathcal{E}} \boldsymbol{f}_k \Big(E_{\Delta t/2}^{bilin} R_\hbar \boldsymbol{U}^n + E_{\Delta t/2}^{const}(1-\mu_x^2\mu_y^2)\boldsymbol{U}^n \Big) \mathrm{d}S, \tag{2.4}$$

where $\mu_x^2 U_{ij} = 1/4(U_{i+1,j}+2U_{ij}+U_{i-1,j})$; an analogous notation is used for the $y-$direction. It has been shown in [22] that the combination (2.4) yields the best results with respect to accuracy as well as stability among other possible second order FVEG schemes. It is particularly interesting that the constant evolution term $E_{\Delta t/2}^{const}(1-\mu_x^2\mu_y^2)\boldsymbol{U}^n$ that corrects the conservativity of the intermediate solutions along cell-interfaces is very important; if it is not used the scheme is second order formally, but unconditionally unstable, cf. the FVEG-B scheme [22].

In what follows we will describe the well-balanced approximation of the source term in the finite volume update step; we will proof in the Section 4, that it is the approximation that preserves stationary steady states as well as the steady jets in the rotational frame, cf. Theorems 4.1 and 4.2. Many geophysical flows are nearly hydrostatic, i.e. $\sqrt{u^2+v^2} << \sqrt{gh}$. In the associated asymptotic limit the leading order water height h satisfies the balance of momentum flux and momentum source terms. In particular, this leads to the following stationary state of (2.1) $u = 0 = v$ and $h + b =$ const., which is the so-called lake at rest state.
If the effect of the Coriolis forces is included the situation is more complicated. Assume no dependence in $y-$direction in (2.1). Then $u = 0$, $gh\partial_x(h+b) = fhv$ is an exact steady solution of this shallow water system. This yields the following balance condition $gh(h+b+C)_x = 0$, where C is the primitive to $-fv/g$.
The source term $\boldsymbol{B}_{ij}^{n+1/2}$ will be approximated in the so-called interface-based way in order to reflect a delicate balance between the gradient of flux functions and the right-hand-side source term for stationary and steady or quasi-steady states, cf. [27]. For both equilibrium states mentioned above the flux differences on cell-interfaces give, e.g. in the second equation of (2.2) yields,

$$\begin{aligned}\frac{g}{2\hbar^2}\int_{y_{i-1/2}}^{y_{i+1/2}} \Big((h_{i+1/2}^{n+1/2})^2 - (h_{i-1/2}^{n+1/2})^2 \Big)\, \mathrm{d}S_y \\ = \frac{g}{2\hbar^2}\int_{y_{i-1/2}}^{y_{i+1/2}} \Big(h_{i+1/2}^{n+1/2} + h_{i-1/2}^{n+1/2} \Big) \Big(h_{i+1/2}^{n+1/2} - h_{i-1/2}^{n+1/2} \Big)\, \mathrm{d}S_y.\end{aligned} \tag{2.5}$$

The approximation of the primitive to the Coriolis forces can be constructed in the following way

$$C_{i+1/2}^{n+1/2} = -\frac{f}{g}\hbar \sum_{i'=i_0}^{i} \frac{v_{i'-1/2}^{n+1/2} + v_{i'+1/2}^{n+1/2}}{2}, \quad i \in \mathbb{Z}.$$

here $i_0 \in \mathbb{Z}$ is a suitable starting index; e.g. $i_0 = 1$; the discretization of the primitive of the Coriolis forces in the $y-$ direction is analogous

$$D_{j+1/2}^{n+1/2} = \frac{f}{g}\hbar \sum_{j'=j_0}^{j} \frac{u_{j'-1/2}^{n+1/2} + u_{j'+1/2}^{n+1/2}}{2}, \quad j \in \mathbb{Z}.$$

Since $gh(h+b+C)_x = 0$, the formula (2.5) already dictates the well-balanced approximation of the source term

$$\frac{1}{\hbar^2}\int_{\Omega_{ij}} B_2(\boldsymbol{U}^{n+1/2}) = \frac{1}{\hbar^2}\int_{x_{i-1/2}}^{x_{i+1/2}}\int_{y_{i-1/2}}^{y_{i+1/2}} -gh^{n+1/2}(b_x^{n+1/2}+C_x^{n+1/2}) \tag{2.6}$$
$$\approx \frac{-g}{\hbar}\int_{y_{i-1/2}}^{y_{i+1/2}} \frac{h_{i+1/2}^{n+1/2}+h_{i-1/2}^{n+1/2}}{2}\,\frac{(b_{i+1/2}+C_{i+1/2}^{n+1/2})-(b_{i-1/2}+C_{i-1/2}^{n+1/2})}{\hbar}\mathrm{d}S_y.$$

Integration along the vertical edge, i.e. from $y_{i-1/2}$ to $y_{i+1/2}$, is done analogously to the cell-interface integration of fluxes in (2.5) by the Simpson rule.

3 Well-balanced approximate evolution operators

We believe that the most satisfying methods for evolutionary problems are based on the approximation of evolution operator or at least its dominant part. In order to derive the exact integral equations, which describe time evolution of the solution of the shallow water equations, we rewrite first (2.1) in primitive variables

$$\boldsymbol{w}_t + \boldsymbol{A}_1(\boldsymbol{w})\boldsymbol{w}_x + \boldsymbol{A}_2(\boldsymbol{w})\boldsymbol{w}_y = \boldsymbol{t}(\boldsymbol{w}), \tag{3.1}$$

$$\boldsymbol{w} = \begin{pmatrix} h \\ u \\ v \end{pmatrix}, \boldsymbol{A}_1 = \begin{pmatrix} u & h & 0 \\ g & u & 0 \\ 0 & 0 & u \end{pmatrix}, \boldsymbol{A}_2 = \begin{pmatrix} v & 0 & h \\ 0 & v & 0 \\ g & 0 & v \end{pmatrix}, \boldsymbol{t} = \begin{pmatrix} 0 \\ -gb_x + fv \\ -gb_y - fu \end{pmatrix}.$$

The homogeneous part of (3.1) yields a hyperbolic system. Its matrix pencil $\boldsymbol{A} = \boldsymbol{A}_1\cos\theta + \boldsymbol{A}_2\sin\theta$, has three eigenvalues

$$\begin{aligned} \lambda_1 &= u\cos\theta + v\sin\theta - c, \\ \lambda_2 &= u\cos\theta + v\sin\theta, \\ \lambda_3 &= u\cos\theta + v\sin\theta + c, \end{aligned}$$

and a full set of right eigenvectors

$$\boldsymbol{r}_1 = \begin{pmatrix} -1 \\ g/c\cos\theta \\ g/c\sin\theta \end{pmatrix}, \ \boldsymbol{r}_2 = \begin{pmatrix} 0 \\ \sin\theta \\ -\cos\theta \end{pmatrix}, \ \boldsymbol{r}_3 = \begin{pmatrix} 1 \\ g/c\cos\theta \\ g/c\sin\theta \end{pmatrix},$$

where $c = \sqrt{gh}$ denotes the wave celerity. The eigenvalues $\lambda_{1,3}$ correspond to fast waves, the so-called inertia-gravity waves, whereas slow modes are related to λ_2. Analogously to the gas dynamics the Froude number $Fr = |\boldsymbol{u}|/c$ plays an important role in the classification of shallow flows. The shallow flow is called supercritical, critical or subcritical for $Fr > 1, Fr = 1$, and $Fr < 1$, respectively.
Now we linearize (3.1) by freezing the Jacobian matrices at a suitable local state $\tilde{h}, \tilde{u}, \tilde{v}$. This linearized local states are computed as local averages at the quadrature points for cell interface flux integrals. In computations presented here the Simpson rule for cell-interface integrals is used and thus the linearization is applied locally at vertices of mesh cells and midpoints of cell interfaces. Applying the theory of bicharacteristics to (3.1) yields the exact integral equations in an analogous way as in [22]

$$
\begin{aligned}
h\left(P\right) &= \frac{1}{2\pi}\int_0^{2\pi} h\left(Q\right) - \frac{\tilde{c}}{g}u\left(Q\right)\cos\theta - \frac{\tilde{c}}{g}v\left(Q\right)\sin\theta \mathrm{d}\theta \\
&-\frac{1}{2\pi}\int_{t_n}^{t_{n+1}} \frac{1}{t_{n+1}-\tilde{t}}\int_0^{2\pi}\frac{\tilde{c}}{g}\Big(u(\tilde{Q})\cos\theta + v(\tilde{Q})\sin\theta\Big)\,\mathrm{d}\theta\mathrm{d}\tilde{t} \\
&+\frac{1}{2\pi}\tilde{c}\int_{t_n}^{t_{n+1}}\int_0^{2\pi}\Big(b_x(\tilde{Q})\cos\theta + b_y(\tilde{Q})\sin\theta\Big)\,\mathrm{d}\theta\mathrm{d}\tilde{t} \\
&-\frac{1}{2\pi}\frac{\tilde{c}f}{g}\int_{t_n}^{t_{n+1}}\int_0^{2\pi}\Big(v(\tilde{Q})\cos\theta - u(\tilde{Q})\sin\theta\Big)\,\mathrm{d}\theta\mathrm{d}\tilde{t},
\end{aligned}
\tag{3.2}
$$

$$
\begin{aligned}
u\left(P\right) &= \frac{1}{2}u\left(Q_0\right) + \frac{1}{2\pi}\int_0^{2\pi} -\frac{g}{\tilde{c}}h\left(Q\right)\cos\theta + u\left(Q\right)\cos^2\theta + v\left(Q\right)\sin\theta\cos\theta\,\mathrm{d}\theta \\
&-\frac{g}{2}\int_{t_n}^{t_{n+1}}\Big(h_x(\tilde{Q}_0) + b_x(\tilde{Q}_0)\Big)\,\mathrm{d}\tilde{t} \\
&-\frac{g}{2\pi}\int_{t_n}^{t_{n+1}}\int_0^{2\pi}\Big(b_x(\tilde{Q})\cos^2\theta + b_y(\tilde{Q})\sin\theta\cos\theta\Big)\,\mathrm{d}\theta\mathrm{d}\tilde{t} \\
&+\frac{1}{2\pi}\int_{t_n}^{t_{n+1}}\frac{1}{t_{n+1}-\tilde{t}}\int_0^{2\pi}\Big(u(\tilde{Q})\cos 2\theta + v(\tilde{Q})\sin 2\theta\Big)\,\mathrm{d}\theta\mathrm{d}\tilde{t} \\
&+\frac{f}{2}\int_{t_n}^{t_{n+1}} v(\tilde{Q}_0)\mathrm{d}\tilde{t} + \frac{f}{2\pi}\int_{t_n}^{t_{n+1}}\int_0^{2\pi}\Big(v(\tilde{Q})\cos^2\theta - u(\tilde{Q})\sin\theta\cos\theta\Big)\,\mathrm{d}\theta\mathrm{d}\tilde{t},
\end{aligned}
\tag{3.3}
$$

$$
\begin{aligned}
v\left(P\right) &= \frac{1}{2}v\left(Q_0\right) + \frac{1}{2\pi}\int_0^{2\pi} -\frac{g}{\tilde{c}}h\left(Q\right)\sin\theta + u\left(Q\right)\sin\theta\cos\theta + v\left(Q\right)\sin^2\theta\,\mathrm{d}\theta \\
&-\frac{g}{2}\int_{t_n}^{t_{n+1}}\Big(h_y(\tilde{Q}_0) + b_y(\tilde{Q}_0)\Big)\,\mathrm{d}\tilde{t} \\
&-\frac{g}{2\pi}\int_{t_n}^{t_{n+1}}\int_0^{2\pi}\Big(b_x(\tilde{Q})\sin\theta\cos\theta + b_y(\tilde{Q})\sin^2\theta\Big)\,\mathrm{d}\theta\mathrm{d}\tilde{t} \\
&+\frac{1}{2\pi}\int_{t_n}^{t_{n+1}}\frac{1}{t_{n+1}-\tilde{t}}\int_0^{2\pi}\Big(u(\tilde{Q})\sin 2\theta - v(\tilde{Q})\cos 2\theta\Big)\,\mathrm{d}\theta\mathrm{d}\tilde{t} \\
&-\frac{f}{2}\int_{t_n}^{t_{n+1}} u(\tilde{Q}_0)\mathrm{d}\tilde{t} + \frac{f}{2\pi}\int_{t_n}^{t_{n+1}}\int_0^{2\pi}\Big(v(\tilde{Q})\sin\theta\cos\theta - u(\tilde{Q})\sin^2\theta\Big)\,\mathrm{d}\theta\mathrm{d}\tilde{t}.
\end{aligned}
\tag{3.4}
$$

Evolution takes place along the bicharacteristic cone, see Fig. 1, where $P = (x, y, t_{n+1})$ is the peak of the bicharacteristic cone, $Q_0 = (x - \tilde{u}\Delta t, y - \tilde{v}\Delta t, t_n)$ denotes the center of the sonic circle, $\tilde{Q}_0 = (x - \tilde{u}(t_n + \Delta t - \tilde{t}), y - \tilde{v}(t_n + \Delta t - \tilde{t}), \tilde{t})$, $\tilde{Q} = (x - \tilde{u}(t_n + \Delta t - \tilde{t}) + c(t_n + \Delta t - \tilde{t})\cos\theta, y - \tilde{v}(t_n + \Delta t - \tilde{t}) + c(t_n + \Delta t - \tilde{t})\sin\theta, \tilde{t})$ stays for arbitrary point on the mantle and $Q = Q(\tilde{t})\Big|_{\tilde{t}=t_n}$ denotes a point at the perimeter of the sonic circle at time t_n. Now, in order to construct a well-balanced FVEG scheme the balance between source terms and gradients of fluxes needs to be reflected also in the approximate evolution operator. In the next lemma the well balanced approximation of (3.2) - (3.4) is derived.

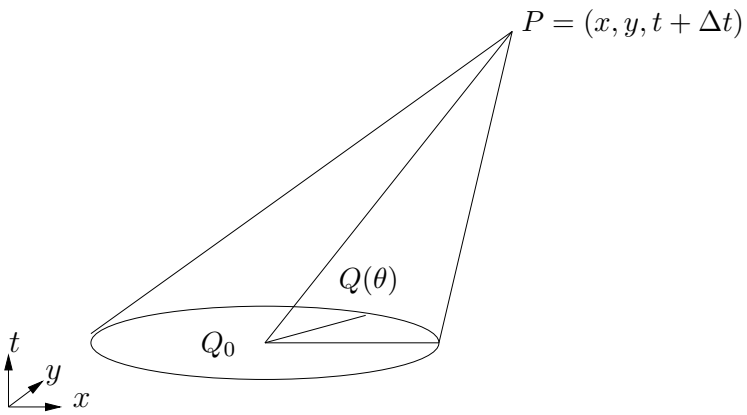

Figure 1: Bicharacteristics cone created by bicharacteristics through P and $Q = Q(\theta)$.

Lemma 3.1 *The well-balanced approximation of the exact integral equations (3.2)- (3.4) reads*

$$\begin{aligned} h(P) &= -b(P) + \frac{1}{2\pi}\int_0^{2\pi} (h(Q) + b(Q)) - \frac{\tilde{c}}{g} u(Q)\cos\theta - \frac{\tilde{c}}{g} v(Q)\sin\theta\, d\theta \qquad (3.5) \\ &\quad -\frac{1}{2\pi}\int_{t_n}^{t_{n+1}} \frac{1}{t_{n+1}-\tilde{t}} \int_0^{2\pi} \frac{\tilde{c}}{g}\left(u(\tilde{Q})\cos\theta + v(\tilde{Q})\sin\theta\right) d\theta\, d\tilde{t} + O\left(\Delta t^2\right), \end{aligned}$$

$$\begin{aligned} u(P) &= \frac{1}{2\pi}\int_0^{2\pi} -\frac{g}{\tilde{c}} (h(Q) + b(Q) + C(Q))\cos\theta + u(Q)\cos^2\theta + v(Q)\sin\theta\cos\theta\, d\theta \\ &\quad +\frac{1}{2}u(Q_0) - \frac{1}{2\pi}\int_{t_n}^{t_{n+1}} \frac{1}{t_{n+1}-\tilde{t}} \int_0^{2\pi} \frac{g}{\tilde{c}}\left(h(\tilde{Q}) + b(\tilde{Q}) + C(\tilde{Q})\right)\cos\theta\, d\theta\, d\tilde{t} \quad (3.6) \\ &\quad +\frac{1}{2\pi}\int_{t_n}^{t_{n+1}} \frac{1}{t_{n+1}-\tilde{t}} \int_0^{2\pi} \left(u(\tilde{Q})\cos 2\theta + v(\tilde{Q})\sin 2\theta\right) d\theta\, d\tilde{t} + O\left(\Delta t^2\right), \end{aligned}$$

$$\begin{aligned} v(P) &= \frac{1}{2\pi}\int_0^{2\pi} -\frac{g}{\tilde{c}} (h(Q) + b(Q) + D(Q))\sin\theta + u(Q)\sin\theta\cos\theta + v(Q)\sin^2\theta\, d\theta \\ &\quad +\frac{1}{2}v(Q_0) - \frac{1}{2\pi}\int_{t_n}^{t_{n+1}} \frac{1}{t_{n+1}-\tilde{t}} \int_0^{2\pi} \frac{g}{\tilde{c}}\left(h(\tilde{Q}) + b(\tilde{Q}) + D(\tilde{Q})\right)\sin\theta\, d\theta\, d\tilde{t} \quad (3.7) \\ &\quad +\frac{1}{2\pi}\int_{t_n}^{t_{n+1}} \frac{1}{t_{n+1}-\tilde{t}} \int_0^{2\pi} \left(u(\tilde{Q})\sin 2\theta - v(\tilde{Q})\cos 2\theta\right) d\theta\, d\tilde{t} + O\left(\Delta t^2\right). \end{aligned}$$

Remark 3.1 It is easy to see that the approximations (3.5)-(3.7) are well-balanced in the sense that the stationary steady equilibrium state, $u = 0 = v$ and $h + b =$ const., is preserved exactly. An important property of the evolution operator (3.5)-(3.7) is that the bottom elevation, the depth of the water and the primitives to the Coriolis forces are represented by analogous terms. In the Section 4 we will prove that the whole FVEG scheme is well-balanced for steady stationary states as well as for steady jets in the rotational frame.

Proof: We show that the approximate integral equations (3.5)-(3.7) are consistent with the exact integral equations (3.2)-(3.4). In (3.2) the integral with bottom topography

terms can be rewritten using the polar coordinates $x = r\cos\theta$, $y = r\sin\theta$

$$\begin{aligned}\frac{\tilde{c}}{2\pi}\int_{t_n}^{t_{n+1}}\int_0^{2\pi}\Big(b_x(\tilde{Q})\cos\theta + b_y(\tilde{Q})\sin\theta\Big)\,\mathrm{d}\theta\mathrm{d}\tilde{t} &= \frac{\tilde{c}}{2\pi}\int_{\tilde{c}\Delta t}^{0}\int_0^{2\pi}\frac{\mathrm{d}b(r,\theta)}{\mathrm{d}r}\mathrm{d}\theta(-\frac{\mathrm{d}r}{\tilde{c}})\\ = \int_0^{\tilde{c}\Delta t}\frac{\mathrm{d}}{\mathrm{d}r}\left(\frac{1}{2\pi}\int_0^{2\pi} b\,\mathrm{d}\theta\right)\mathrm{d}r &= \frac{1}{2\pi}\int_0^{2\pi} b(Q)\mathrm{d}\theta - b(P), \qquad (3.8)\end{aligned}$$

which yields the corresponding terms in (3.5). Further, we show that the integrals in (3.2) obtaining the Coriolis forces are of order $O(\Delta t^2)$. Applying the rectangle rule in time and the Taylor expansion in the center of the sonic circle Q_0 yield

$$\begin{aligned}&\int_{t_n}^{t_{n+1}}\int_0^{2\pi} v(\tilde{Q})\cos\theta\mathrm{d}\theta\mathrm{d}\tilde{t} = \Delta t\int_0^{2\pi} v(Q)\cos\theta\mathrm{d}\theta + O(\Delta t^2) =\\ &\Delta t\int_0^{2\pi} v(Q_0)\cos\theta + c\Delta t\, v_x(Q_0)\cos^2\theta + c\Delta t\, v_y(Q_0)\cos\theta\sin\theta + O(\Delta t^2)\mathrm{d}\theta =\\ &O(\Delta t^2) \qquad (3.9)\end{aligned}$$

with an analogous approximation for the Coriolis forces in y-direction. This yields together with (3.8) and (3.9) the approximate integral equation (3.5).
In the equation (3.3) for velocity u we apply for the mantle integrals containing the bottom elevation terms the rectangle rule in time and the Taylor expansion over the center Q_0 of the sonic circle at time t_n, which lead to

$$\frac{1}{2\pi}g\int_{t_n}^{t_{n+1}}\int_0^{2\pi}\Big(b_x(\tilde{Q})\cos\theta + b_y(\tilde{Q})\sin\theta\Big)\cos\theta\ \mathrm{d}\theta\,\mathrm{d}\tilde{t} = \frac{g\Delta t}{2}b_x(Q_0) + O(\Delta t^2). \qquad (3.10)$$

To complete we eliminate derivative by replacing the term $b_x(Q_0)$ by its average over the sonic circle O and applying the Gauss theorem

$$b_x(Q_0) = \frac{1}{\pi\tilde{c}^2\Delta t^2}\int_O b_x(Q)\,\mathrm{d}x\mathrm{d}y + O(\Delta t^2) = \frac{1}{\pi\tilde{c}\Delta t}\int_0^{2\pi} b(Q)\cos\theta\,\mathrm{d}\theta + O(\Delta t^2), \quad (3.11)$$

which after the substitution into (3.10) yields

$$\frac{1}{2\pi}g\int_{t_n}^{t_{n+1}}\int_0^{2\pi}\Big(b_x(\tilde{Q})\cos\theta + b_y(\tilde{Q})\sin\theta\Big)\cos\theta\ \mathrm{d}\theta\,\mathrm{d}\tilde{t} = \frac{g}{\tilde{c}}\frac{1}{2\pi}\int_0^{2\pi} b(Q)\cos\theta\,\mathrm{d}\theta + O(\Delta t^2). \qquad (3.12)$$

Rewriting the Coriolis forces terms using their primitives we obtain analogously to (3.10) and (3.11)

$$\begin{aligned}&\frac{f}{2\pi}\int_{t_n}^{t_{n+1}}\int_0^{2\pi}\Big(v(\tilde{Q})\cos^2\theta - u(\tilde{Q})\sin\theta\cos\theta\Big)\,\mathrm{d}\theta\mathrm{d}\tilde{t} \qquad (3.13)\\ &= -\frac{g}{2\pi}\int_{t_n}^{t_{n+1}}\int_0^{2\pi}\Big(C_x(\tilde{Q})\cos\theta + D_y(\tilde{Q})\sin\theta\Big)\cos\theta\ \mathrm{d}\theta\,\mathrm{d}\tilde{t}\\ &= -\frac{g}{\tilde{c}}\frac{1}{2\pi}\int_0^{2\pi} C(Q)\cos\theta\,\mathrm{d}\theta + O(\Delta t^2).\end{aligned}$$

This balances together with (3.12) the analogous term with $h(Q)\cos\theta$ in (3.3). Integral along the middle bicharacteristic

$$\frac{g}{2}\int_{t_n}^{t_{n+1}}\left(h_x(\tilde{Q}_0)+b_x(\tilde{Q}_0)-\frac{f}{g}v(\tilde{Q}_0)\right)\mathrm{d}\tilde{t}=\frac{g}{2}\int_{t_n}^{t_{n+1}}\left(h_x(\tilde{Q}_0)+b_x(\tilde{Q}_0)+C_x(\tilde{Q}_0)\right)\mathrm{d}\tilde{t}$$

can be approximated in a similar way as (3.11) applying the Gauss theorem at each intermediate circular section at $\tilde{t}$ along the mantle of the bicharacteristic cone. Substituting into (3.3) gives (3.6). Approximation (3.7) for the velocity v is obtained in an analogous way as (3.6).

□

Remark 3.2 It should be pointed out that if the primitives to the Coriolis forces are equal, i.e. $C = D$, then the fact that $C_{xy} = D_{yx}$ yields $-\frac{f}{g}v_y = \frac{f}{g}u_x$. Thus div $\underline{\mathrm{u}} = 0$, where $\underline{\mathrm{u}}$ is the velocity vector (u, v).
In this case the influence of the Coriolis forces can be directly imbedded into the integral equation for $h(P)$ in an analogous way to the bottom topography integrals in (3.8). The resulting integral equation for the water depth h then reads

$$\begin{aligned} h\,(P) \;=\; & -(b(P)+C(P)) \\ & +\frac{1}{2\pi}\int_0^{2\pi}\left(h\,(Q)+b\,(Q)+C\,(Q)\right)-\frac{\tilde{c}}{g}\left(u\,(Q)\cos\theta+v\,(Q)\sin\theta\right)\mathrm{d}\theta \\ & -\frac{1}{2\pi}\int_{t_n}^{t_{n+1}}\frac{1}{t_{n+1}-\tilde{t}}\int_0^{2\pi}\frac{\tilde{c}}{g}\left(u(\tilde{Q})\cos\theta+v(\tilde{Q})\sin\theta\right)\mathrm{d}\theta\mathrm{d}\tilde{t}+O\left(\Delta t^2\right). \end{aligned} \tag{3.14}$$

Our next aim is to derive an approximate evolution operator which is explicit in time. Therefore, the next step is to approximate in (3.5) - (3.7) the so-called mantle integrals, i.e. $\int_{t_n}^{t_{n+1}}\frac{1}{t_n-\tilde{t}}\int_0^{2\pi}\mathrm{d}\theta\mathrm{d}\tilde{t}$, by suitable numerical quadratures. This problem has been extensively studied in [17], [18], [22] for linear wave equation system, for the shallow water equations as well as for the Euler equations of gas dynamics. It has been shown that classical quadratures, such as the rectangle rule, the trapezoidal rule, etc., are not well suited for approximation of discontinuous waves, which may propagate along the mantle of the bicharacteristic cone. It resulted in a reduced stability range of the FVEG. For example, if the mantle time integrals are approximated by the rectangle rule the CFL stability number was 0.63 and 0.56 for the first and second order FVEG scheme, respectively; it is the so-called FVEG3 scheme, cf. [19]. In the recent paper [22] new quadrature rules have been proposed for the mantle integrals. As a result new approximate evolution operators evaluate exactly each planar wave propagating either in $x-$ or $y-$ directions and increase the stability range of the FVEG scheme substantially yielding the CFL number close to 1. The numerical quadratures were proposed separately for constant and (bi-)linear approximations and will be now used systematically in order to approximate all time integrals in (3.5)-(3.7). For example, if $f = f(x)$ is a piecewise constant function, then it was shown in [22] that

$$\int_0^{2\pi}f(Q)\cos\theta\mathrm{d}\theta+\int_{t_n}^{t_{n+1}}\frac{1}{t_n-\tilde{t}}\int_0^{2\pi}f(\tilde{Q})\cos\theta\mathrm{d}\tilde{t}=\int_0^{2\pi}f(Q)\ \mathrm{sgn}\cos\theta\mathrm{d}\theta,$$

an analogous relation holds for $f(Q)\sin\theta$.

Thus, following [22] we get for piecewise constant approximate functions the approximate evolution operator E_Δ^{const}

$$\begin{aligned}
h(P) &= -b(P) + \frac{1}{2\pi}\int_0^{2\pi}\left[(h(Q)+b(Q)) - \frac{\tilde{c}}{g}u(Q)\,\mathrm{sgn}(\cos\theta) - \frac{\tilde{c}}{g}v(Q)\,\mathrm{sgn}(\sin\theta)\right]\mathrm{d}\theta \\
u(P) &= \frac{1}{2\pi}\int_0^{2\pi}\Big[-\frac{g}{\tilde{c}}(h(Q)+b(Q)+C(Q))\,\mathrm{sgn}(\cos\theta) + u(Q)\left(\cos^2\theta+\frac{1}{2}\right) \\
&\qquad + v(Q)\sin\theta\cos\theta\Big]d\theta \\
v(P) &= \frac{1}{2\pi}\int_0^{2\pi}\Big[-\frac{g}{\tilde{c}}(h(Q)+b(Q)+D(Q))\,\mathrm{sgn}(\sin\theta) + u(Q)\sin\theta\cos\theta \\
&\qquad + v(Q)\left(\sin^2\theta+\frac{1}{2}\right)\Big]d\theta. \qquad (3.15)
\end{aligned}$$

If the continuous piecewise bilinear ansatz functions are used we obtain in an analogous way as in [22] the approximate evolution operator E_Δ^{bilin}

$$\begin{aligned}
h(P) &= -b(P) + h(Q_0) + b(Q_0) + \frac{1}{4}\int_0^{2\pi}(h(Q)-h(Q_0)) + (b(Q)-b(Q_0))\mathrm{d}\theta \\
&\quad -\frac{1}{\pi}\int_0^{2\pi}\left[\frac{\tilde{c}}{g}u(Q)\cos\theta + \frac{\tilde{c}}{g}v(Q)\sin\theta\right]\mathrm{d}\theta \\
u(P) &= u(Q_0) - \frac{1}{\pi}\int_0^{2\pi}\frac{g}{\tilde{c}}(h(Q)+b(Q)+C(Q))\cos\theta\mathrm{d}\theta \\
&\quad +\frac{1}{4}\int_0^{2\pi}\left[3u(Q)\cos^2\theta + 3v(Q)\sin\theta\cos\theta - u(Q) - \frac{1}{2}u(Q_0)\right]\mathrm{d}\theta \\
v(P) &= v(Q_0) - \frac{1}{\pi}\int_0^{2\pi}\frac{g}{\tilde{c}}(h(Q)+b(Q)+D(Q))\sin\theta\mathrm{d}\theta \\
&\quad +\frac{1}{4}\int_0^{2\pi}\left[3u(Q)\sin\theta\cos\theta + 3v(Q)\sin^2\theta - v(Q) - \frac{1}{2}v(Q_0)\right]\mathrm{d}\theta. \qquad (3.16)
\end{aligned}$$

These operators are used in (2.3) and (2.4) to compute the intermediate solution at time $t_n + \Delta t/2$ in order to evolve fluxes along cell interfaces.

4 The well-balanced FVEG scheme

In this section we first summarize the main steps of the FVEG method by presenting the algorithm for the first and second order scheme including the effects of bottom topography as well as the Coriolis forces. Further, we prove the well-balanced behaviour of the FVEG scheme for stationary steady states and for steady jets on the rotating plane.

4.1 Algorithm

1 Given are piecewise constant approximations at time t_n: $h_{ij}^n, u_{ij}^n, v_{ij}^n, i,j \in \mathbb{Z}$, the bottom topography $b(x,y)$, mesh and time steps $\hbar, \Delta t$ and constants g, f; compute

$$b_{ij}^n = b(x_i, y_j, t^n),$$

$$C_{ij}^n = -\frac{f}{g}\hbar \sum_{i'=i_0}^{i} \frac{v_{i'-1,j}^n + v_{i'j}^n}{2},$$
$$D_{ij}^n = \frac{f}{g}\hbar \sum_{j'=j_0}^{j} \frac{u_{i,j'-1}^n + u_{ij'}^n}{2}.$$

2 *recovery step:*
If the scheme is second order, do the recovery step and apply the limiter procedure, e.g. by using the minmod limiter; cf. [21]. This yields the piecewise bilinear approximations $R_\hbar h^n$, $R_\hbar u^n$, $R_\hbar v^n$, $R_\hbar b^n$, $R_\hbar C^n$, $R_\hbar D^n$.

3 *predictor step / approximate evolution:*
Compute the intermediate solutions at time level $t_{n+1/2}$ on the cell interfaces by the approximate evolution operators. For the first order scheme use (2.3) and (3.15); the second order scheme is computed using (2.4) and (3.15), (3.16). Integration along the cell interfaces is realized numerically by the Simpson rule.

4 *corrector step / FV-update:*
Compute the Coriolis forces and the bottom topography at the intermediate time level $t_{n+1/2}$ and at each integration points on cell interfaces, i.e. at vertices and midpoints:

$$b_{k\ell}^{n+1/2} = b(x_k, y_\ell), \quad k = i, i \pm 1/2,\ \ell = j, j \pm 1/2;$$
$$C_{i+1/2,\ell}^{n+1/2} = -\frac{f}{g}\hbar \sum_{i'=i_0}^{i} \frac{v_{i-1/2,\ell}^{n+1/2} + v_{i+1/2,\ell}^{n+1/2}}{2}, \quad \ell = j, j \pm 1/2;$$
$$D_{k,j+1/2}^{n+1/2} = \frac{f}{g}\hbar \sum_{j'=j_0}^{j} \frac{u_{k,j-1/2}^{n+1/2} + u_{kj+1/2}^{n+1/2}}{2}, \quad k = i, i \pm 1/2.$$

Do the FV-update (2.2) using the well-balanced approximation of the source terms (2.6).

4.2 Theoretical analysis of the well-balanced properties

In what follows the well-balanced property of the FVEG scheme will be proven for two cases; for the stationary steady states as well as for the steady jets in the rotational frame.

Theorem 4.1 *The FVEG method is well-balanced for the lake at rest, i.e. the stationary steady states $u = 0 = v$ and $K := h + b + C = const.$, $L := h + b + D = const.$ are preserved. More precisely we have for all cells Ω_{ij}, $i, j \in \mathbb{Z}$*

i) if $u^n = 0 = v^n, K^n = \overline{K} = const., L^n = \overline{L} = const.$, then $u^{n+1/2} = 0 = v^{n+1/2}$, $K^{n+1/2} = \overline{K}, L^{n+1/2} = \overline{L}$.

ii) if $u^{n+1/2} = 0 = v^{n+1/2}, K^{n+1/2} = \overline{K}, L^{n+1/2} = \overline{L}$, then $u^{n+1} = 0 = v^{n+1}$, $K^{n+1} = \overline{K}, L^{n+1} = \overline{L}$.

Proof:
i) Assuming the stationary situation, i.e. $u^n = 0 = v^n$, we have from the first equation

of the approximate evolution operator (3.15) that the water level $h+b$ is flat

$$h^{n+1/2}(P)+b^{n+1/2}(P)=\frac{1}{2\pi}\int_0^{2\pi}(h^n(Q)+b^n(Q))\mathrm{d}\theta=\text{const.}$$

For better readability we express explicitly time dependence here. Further, we have from the evolution equation (3.15) for velocity that

$$u^{n+1/2}(P)=\frac{1}{2\pi}\int_0^{2\pi}-\frac{g}{\tilde{c}}(h^n(Q)+b^n(Q)+C^n(Q))\,\mathrm{sgn}(\cos\theta).$$

Since $K^n=h^n+b^n+C^n=$ const., we get $u^{n+1/2}=0$; the analogous relation holds for $v^{n+1/2}$ in the y-direction, too.
Further, it is easy to see that $K^{n+1/2}=\overline{K}$. Let P be an integration point at the cell interface $\mathcal{E}_{i+1/2,j}$, i.e. $P=(x_{i+1/2},y_k)$, $k=j\pm 1/2, j$. Then we obtain that

$$\begin{aligned}K^{n+1/2}(P) &= h^{n+1/2}(P)+b^{n+1/2}(P)+C^{n+1/2}(P)\\ &= -b^{n+1/2}(P)+\frac{1}{2\pi}\int_0^{2\pi}(h^n(Q)+b^n(Q))\mathrm{d}\theta+b^{n+1/2}(P)\\ &\quad -\frac{f}{g}\hbar\sum_{i'=i_0}^{i}\frac{v^{n+1/2}_{i'-1/2,k}+v^{n+1/2}_{i'+1/2,k}}{2}=\frac{1}{2\pi}\int_0^{2\pi}K^n(Q)\mathrm{d}\theta=\overline{K}.\end{aligned}$$

In an analogous way the preservation of $L^{n+1/2}=h^{n+1/2}+b^{n+1/2}+D^{n+1/2}$ can be shown. Further, we obtain in the similar way as above that the stationary steady state is preserved also by the approximate evolution operator for piecewise bilinear approximate functions (3.16). Since $u^n=0=v^n$ and $h^n+b^n=$ const. the first equation for the water depth h yields

$$\begin{aligned}h^{n+1/2}(P)+b^{n+1/2}(P) &= h^n(Q_0)+b^n(Q_0)+\frac{1}{4}\int_0^{2\pi}(h^n(Q)-h^n(Q_0)+b^n(Q)-b^n(Q_0))\mathrm{d}\theta\\ &= h^n(Q_0)+b^n(Q_0)=\text{const.}\end{aligned}$$

The other conditions, i.e. $u^{n+1/2}=0=v^{n+1/2}$, $K^{n+1/2}=\overline{K}, L^{n+1/2}=\overline{L}$, can be shown in an analogous way as above.

ii) Assume now that we have at the intermediate time level $t_{n+1/2}$ the stationary steady state, i.e. $u^{n+1/2}=0=v^{n+1/2}, K^{n+1/2}=\overline{K}, L^{n+1/2}=\overline{L}$. Then the first equation for the FV-update of the water depth h yields, cf. (2.2)

$$\begin{aligned}h^{n+1}_{ij} &= h^n_{ij}-\lambda\sum_{k=j,j\pm1/2}\alpha_k((hu)^{n+1/2}_{i+1/2,k}-(hu)^{n+1/2}_{i-1/2,k})-\lambda\sum_{\ell=i,i\pm1/2}\alpha_\ell((hv)^{n+1/2}_{\ell,j+1/2}-(hv)^{n+1/2}_{\ell,j-1/2})\\ &= h^n_{ij},\end{aligned}$$

where α_k, α_ℓ are the integration constants arising from the numerical integration of the flux functions $\boldsymbol{f}_1, \boldsymbol{f}_2$ along the cell interfaces. Using the Simpson rule we have $\alpha_j=4/6, \alpha_{j\pm1}=1/6$ and $\alpha_i=4/6, \alpha_{i\pm1}=1/6$. Since the bottom topography is constant in time, i.e. $b^n=b^{n+1}$, we have shown for the water level that $h^{n+1}+b^{n+1}=$ const. Due to the fact that $u^{n+1/2}=0=v^{n+1/2}$ and $K^{n+1/2}=\overline{K}$, the FV-update for the x-momentum

yields

$$
\begin{aligned}
(hu)_{ij}^{n+1} &= -\lambda \sum_{k=j,j\pm 1/2} \alpha_k \left(\frac{1}{2} g (h^2)_{i+1/2,k}^{n+1/2} - \frac{1}{2} g (h^2)_{i-1/2,k}^{n+1/2} \right) \\
&\quad + \lambda \sum_{k=j,j\pm 1/2} \alpha_k g \frac{h_{i+1/2,k}^{n+1/2} + h_{i+1/2,k}^{n+1/2}}{2} \left((b+C)_{i+1/2,k}^{n+1/2} - (b+C)_{i-1/2,k}^{n+1/2} \right) \\
&= -\lambda \sum_{k=j,j\pm 1/2} \alpha_k g \frac{h_{i+1/2,k}^{n+1/2} + h_{i+1/2,k}^{n+1/2}}{2} \left(K_{i+1/2,k}^{n+1/2} - K_{i-1/2,k}^{n+1/2} \right) = 0. \qquad (4.17)
\end{aligned}
$$

Thus, $u^{n+1} = 0$ and the same holds also for the y-velocity component v^{n+1}. Since $h^{n+1} + b^{n+1} = h^n + b^n = \text{const.}$ and $u^{n+1} = 0 = v^{n+1}$ it is easy to realize that also $K^{n+1} = h^{n+1} + b^{n+1} + C^{n+1} = \overline{K}$ and $L^{n+1} = h^{n+1} + b^{n+1} + D^{n+1} = \overline{L}$, which concludes the proof. □

Theorem 4.2 *The FVEG method is well-balanced for steady jets in the rotational frame, i.e. states $u = 0, v = v(x,t), h = h(x,t)$ and $K := h + b + C = const.$ are preserved. More precisely, we have*

i) if $u^n = 0, K^n := h^n + b^n + C^n = \overline{K} = const.$, $D_y h^n = 0, D_y v^n = 0, D_y b = 0$, for any discrete difference operator D_y in the y-direction, then the same properties hold also on the intermediate time level $t_{n+1/2}$.

ii) if $u^{n+1/2} = 0, K^{n+1/2} = \overline{K}$, $D_y h^{n+1/2} = 0, D_y v^{n+1/2} = 0, D_y b = 0$, then $\boldsymbol{U}^{n+1} = \boldsymbol{U}^n$. In particular, if the assumptions of i) are satisfied, then the same properties hold also on the new time level t_{n+1}.

Proof:
i) We prove here that the approximate evolution operator for piecewise constant data E_Δ^{const}, cf. (3.15), preserves the steady jet, the proof for the approximate evolution operator for piecewise bilinear data E_Δ^{bilin}, cf. (3.16), is analogous.
First, it is easy to see that since $b = b(x)$ and $b_{k\ell}^{n+1/2} = b(x_k, y_\ell)$, then the piecewise constant approximation $b^{n+1/2}$ is also independent on y and $D_y b^{n+1/2} = 0$ for any suitable finite difference operator D_y.
Further, since $u^n = 0, K^n = \overline{K}$ and v^n changes only in the x-direction, we have from the second equation of (3.15) for the velocity u that

$$
\begin{aligned}
u^{n+1/2}(P) &= \frac{1}{2\pi} \int_0^{2\pi} -\frac{g}{\tilde{c}} (h^n(Q) + b^n(Q) + C^n(Q)) \operatorname{sgn}(\cos\theta) + v^n(Q) \sin\theta \cos\theta \mathrm{d}\theta \\
&= \frac{1}{2\pi} \int_0^{2\pi} -\frac{g}{\tilde{c}} \overline{K} \operatorname{sgn}(\cos\theta) \mathrm{d}\theta + \frac{1}{4\pi} \int_{-\pi/2}^{\pi/2} v^R \sin(2\theta) \mathrm{d}\theta \\
&\quad + \frac{1}{4\pi} \int_{\pi/2}^{3\pi/2} v^L \sin(2\theta) \mathrm{d}\theta = 0.
\end{aligned}
$$

We have denoted by v^R and v^L the right and left values of the piecewise constant approximate function v^n to the cell interface $\mathcal{E}_{i+1/2,j}$ obtaining the point P, i.e. P is any of the points $(x_{i+1/2}, y_k)$, $k = j \pm 1/2, j$. Note that due to the CFL stability condition

$\max\{|u+c|\Delta t/\hbar, |v+c|\Delta t/\hbar\} \leq 1$ the base of the sonic circle lies only in the neighbouring cells of the cell interface $\mathcal{E}_{i+1/2,j}$.
The third equation of the approximate evolution operator (3.15) for the velocity v implies

$$\begin{aligned} v^{n+1/2}(P) &= \frac{1}{2\pi}\int_0^{2\pi} -\frac{g}{\tilde{c}}(h^n(Q)+b^n(Q)+D^n(Q))\,\mathrm{sgn}(\sin\theta)+v^n(Q)\left(\sin^2\theta+\frac{1}{2}\right)\mathrm{d}\theta \\ &= -\frac{g}{\tilde{c}}(h^R+b^R)\frac{1}{2\pi}\int_{-\pi/2}^{\pi/2}\mathrm{sgn}(\sin\theta)\mathrm{d}\theta - \frac{g}{\tilde{c}}(h^L+b^L)\frac{1}{2\pi}\int_{\pi/2}^{3\pi/2}\mathrm{sgn}(\sin\theta)\mathrm{d}\theta \\ &\quad +\frac{1}{2}(v^R+v^L) = \frac{1}{2}(v^R+v^L). \end{aligned} \tag{4.18}$$

If $D_y v^n = 0$ it follows from (4.18) that the same holds also on the time level $t_{n+1/2}$, i.e. $D_y v^{n+1/2} = 0$. Further, we have from the first equation of (3.15) for the water depth h that

$$\begin{aligned} K^{n+1/2}(P) &= h^{n+1/2}(P)+b^{n+1/2}(P)+C^{n+1/2}(P) \\ &= \frac{1}{2\pi}\int_0^{2\pi}(h^n(Q)+b^n(Q)) - \frac{\tilde{c}}{g}v^n(Q)\,\mathrm{sgn}(\sin\theta)\mathrm{d}\theta + C^{n+1/2}(P). \end{aligned}$$

Since v^n depends only on x we have $\int_0^{2\pi} v^n(Q)\,\mathrm{sgn}(\sin\theta)\mathrm{d}\theta = 0$ and

$$K^{n+1/2}(P) = \frac{1}{2\pi}\int_0^{2\pi} K^n(Q)\mathrm{d}\theta - \frac{1}{2\pi}\int_0^{2\pi} C^n(Q)\mathrm{d}\theta + C^{n+1/2}(P). \tag{4.19}$$

If we show that

$$C^{n+1/2}(P) = \frac{1}{2\pi}\int_0^{2\pi} C^n(Q)\mathrm{d}\theta, \tag{4.20}$$

then $K^{n+1/2} = \overline{K}$. Denoting $P = (x_{i+1/2}, y_k),\ k = j, j\pm 1/2$, and applying the result from (4.18) lead to

$$\begin{aligned} C^{n+1/2}(P) &= -\frac{f}{g}\hbar\sum_{i'=i_0}^{i}\frac{v^{n+1/2}_{i'-1/2,k}+v^{n+1/2}_{i'+1/2,k}}{2} \\ &= -\frac{f}{g}\hbar\sum_{i'=i_0}^{i}\left(\frac{v^n_{i'-1,k}+v^n_{i',k}}{4}+\frac{v^n_{i',k}+v^n_{i'+1,k}}{4}\right). \end{aligned} \tag{4.21}$$

On the other hand we have

$$\begin{aligned} \frac{1}{2\pi}\int_0^{2\pi} C^n(Q)\mathrm{d}\theta &= \frac{1}{2\pi}\int_{-\pi/2}^{\pi/2}\mathrm{d}\theta\left(-\frac{f}{g}\hbar\sum_{i'=i_0}^{i}\frac{v^{n+1/2}_{i'-1,k}+v^{n+1/2}_{i',k}}{2}\right) \\ &\quad +\frac{1}{2\pi}\int_{\pi/2}^{3\pi/2}\mathrm{d}\theta\left(-\frac{f}{g}\hbar\sum_{i'=i_0}^{i+1}\frac{v^{n+1/2}_{i'-1,k}+v^{n+1/2}_{i',k}}{2}\right), \end{aligned}$$

which is equal to (4.21).
Moreover, the approximate evolution (3.15) for the water depth gives

$$h^{n+1/2}(P) = -b^{n+1/2}(P) + \frac{1}{2\pi}\int_0^{2\pi}(h^n(Q)+b^n(Q))\mathrm{d}\theta,$$

which together with the facts that $D_y h^n = 0$ and $D_y b^{n+1/2} = 0 = D_y b^n$ yields $D_y h^{n+1/2} = 0$.

ii) Now we assume that on the intermediate time level $t_{n+1/2}$ the following conditions hold:

$$u^{n+1/2} = 0, K^{n+1/2} = \overline{K},\ D_y h^{n+1/2} = 0, D_y v^{n+1/2} = 0, D_y b \equiv D_y b^n = 0.$$

The first equation of the finite volume update (2.2) yields

$$h_{ij}^{n+1} = h_{ij}^n - \lambda \sum_{\ell=i,i\pm 1/2} \alpha_\ell ((hv)_{\ell,j+1/2}^{n+1/2} - (hv)_{\ell,j-1/2}^{n+1/2}) = h_{ij}^n,$$

since $D_y h^n = 0$ and $D_y v^n = 0$ for any finite difference operator in the y-direction. Remind that constants α_ℓ arise from the numerical integration along the cell interface.
Since $u^{n+1/2} = 0$, the FV-update for the momentum equation in the x-direction simplifies to

$$\begin{aligned}
(hu)_{ij}^{n+1} &= (hu)_{ij}^n - \lambda \sum_{k=j,j\pm 1/2} \alpha_k \left(\frac{1}{2} g (h^2)_{i+1/2,k}^{n+1/2} - \frac{1}{2} g (h^2)_{i-1/2,k}^{n+1/2} \right) \\
&\quad + \lambda \sum_{k=j,j\pm 1/2} \alpha_k g \frac{h_{i+1/2,k}^{n+1/2} + h_{i+1/2,k}^{n+1/2}}{2} \left((b+C)_{i+1/2,k}^{n+1/2} - (b+C)_{i-1/2,k}^{n+1/2} \right) \\
&= (hu)_{ij}^n - \lambda \sum_{k=j,j\pm 1/2} \alpha_k g \frac{h_{i+1/2,k}^{n+1/2} + h_{i+1/2,k}^{n+1/2}}{2} \left(K_{i+1/2,k}^{n+1/2} - K_{i-1/2,k}^{n+1/2} \right) = (hu)_{ij}^n,
\end{aligned}$$

due to the fact that $K^{n+1/2} = \overline{K}$. In an analogous way we can show for the y-momentum that $(hv)^{n+1/2} = (hv)^n$, which implies $\boldsymbol{U}^n = \boldsymbol{U}^{n+1}$ and concludes the proof. □

5 Numerical experiments

One interesting steady state, which should be correctly resolved by a well-balanced scheme, is the stationary steady state, i.e. $h = $ const. and $u = 0 = v$. In this section we demonstrate well-balanced behaviour of the proposed FVEG schemes through several benchmark problems for stationary and quasi-stationary states, i.e. $h \approx$ const. and $u \approx 0 \approx v$; see [14], [16] for related results in literature. At the end of this section we present results for steady jets including effects of the Coriolis forces and show that the FVEG scheme is well-balanced also for this nontrivial steady state.

5.1 One-dimensional stationary and quasi-stationary states

In this experiment we have tested the preservation of stationary steady state as well as the approximation of small perturbations of this steady state. The bottom topography consists of one hump

$$b(x) = \begin{cases} 0.25(\cos(10\pi(x-0.5)) + 1) & \text{if } |x-0.5| < 0.1 \\ 0 & \text{otherwise} \end{cases}$$

and the initial data are $u(x,0) = 0$,

$$h(x,0) = \begin{cases} 1 - b(x) + \varepsilon & \text{if } 0.1 < x < 0.2 \\ 1 - b(x) & \text{otherwise.} \end{cases}$$

The parameter ε is chosen to be 0, 0.2 or 0.01. The computational domain is the interval $[0, 1]$ and absorbing boundary conditions have been implemented by extrapolating all variables. It should be pointed out that the one-dimensional problems are actually computed by a two-dimensional code by imposing zero tangential velocity $v = 0$.
Firstly we test the ability of the FVEG scheme to preserve the stationary steady state, i.e. the lake at rest case, by taking $\varepsilon = 0$. In Table 1 the L^1-errors for different times computed with the first order FVEG method, cf. (3.15), and with the second order FVEG method, cf. (3.16), are presented. Although we have used a rather coarse mesh consisting of 20×20 mesh cells, it can be seen clearly that the FVEG scheme balances up to the machine accuracy also for long time computations.

Table 1: The L^1-error of the well-balance FVEG scheme using 20×20 mesh cells.

Method	$t = 0.2$	$t = 1$	$t = 10$
first order FVEG	1.110223×10^{-17}	7.216450×10^{-17}	1.332268×10^{-16}
second order FVEG	2.775558×10^{-17}	5.551115×10^{-17}	4.440892×10^{-17}

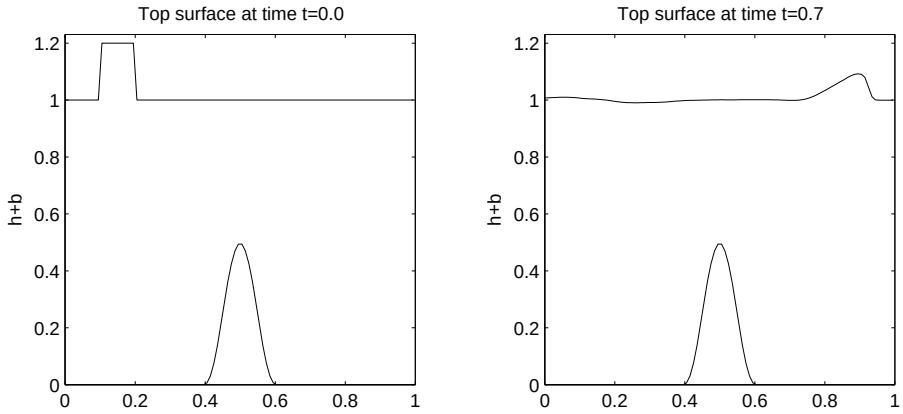

Figure 2: Propagation of small perturbations, $\varepsilon = 0.2$.

In Figure 2 a general behaviour of propagation of small perturbations of the water depth h until time $t = 0.7$ is shown. The solution is computed on a mesh with 100×5 cells and the hight of initial perturbation was $\varepsilon = 0.2$. The initial disturbance generates two waves, the left-going wave runs out of the computational domain, and the right-going wave pasts the bottom elevation obstacle. It is known that if the perturbations are relatively large in comparison to the discretization error a "naive" approximation of the source term, i.e. not well-balanced scheme, e.g. the fractional step method, can still yield reasonable approximations. However, for small perturbations, i.e. ε of order of the discretization errors, such a scheme would yield strong oscillations over the bottom hump and the wave of interest will be lost in the noise, see [16].
In Figure 3 we compare results for water depth h at time $t = 0.7$ obtained by the first and second order FVEG methods using the minmod and monotonized minmod limiters, respectively. On the left picture $\varepsilon = 0.2$, the right picture shows results for $\varepsilon = 0.01$. The reference solutions was obtained by the second order FVEG method with the minmod limiter on a mesh with 10000 cells. We can notice correct resolution of small perturbations

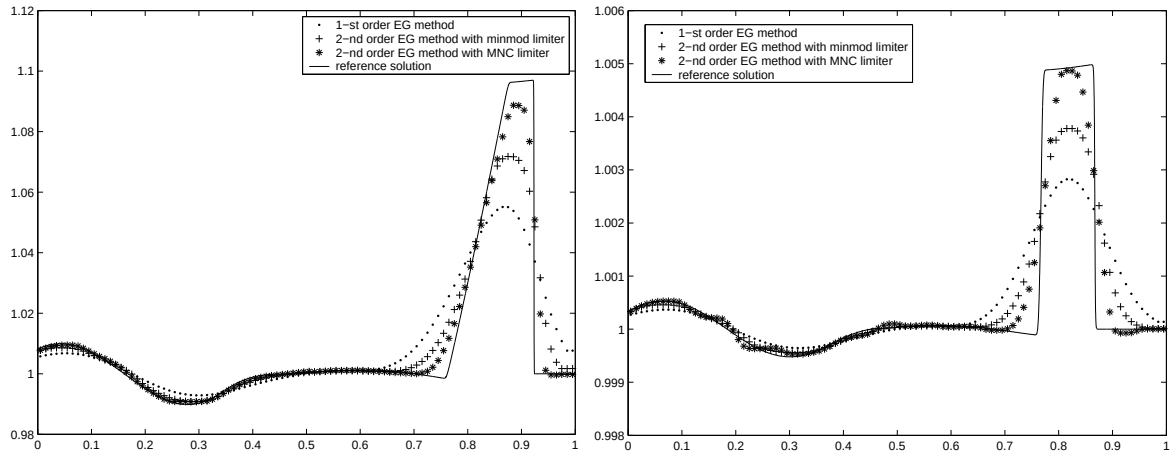

Figure 3: Propagation of small perturbations, magnified view; $\varepsilon = 0.2$ (left) and $\varepsilon = 0.01$ (right).

of the stationary steady state even if the perturbation is of the order of the truncation error.

5.2 Two-dimensional quasi-stationary problem

The second example is a two-dimensional analogy of the previous one. The bottom topography is given by the function

$$b(x,y) \;=\; 0.8\exp\left(-5\,(x-0.9)^2 - 50\,(y-0.5)^2\right) \tag{5.22}$$

and the initial data are

$$\begin{aligned} h(x,y,0) &= \begin{cases} 1-b(x,y)+\varepsilon & \text{if } 0.05 < x < 0.15 \\ 1-b(x,y) & \text{otherwise} \end{cases} \\ u(x,y,0) &= v(x,y,0) = 0. \end{aligned} \tag{5.23}$$

The parameter ε is set to 0.01. The computational domain is $[0,2]\times[0,1]$ and the absorbing extrapolation boundary condition are used. In the Figure 4 we present two solutions computed on a 200×100 grid (left) and on a 600×300 grid (right) by the second order FVEG scheme with the minmod limiter. We can notice that the FVEG method correctly approximate small perturbed waves, the perturbation propagates over the bottom hump without any oscillations. Note that the wave speed is slower over the hump, which leads to a distortion of the initially planar perturbation. The perturbed wave runs out of the computational domain and the flat surface is obtained at the end. Our results are in a good agreement with other results presented in literature, cf., e.g., [14], [16].

5.3 Steady jet in the rotational frame

This is a classical Rossby adjustment of unbalanced jets in an open domain, see, e.g. [5]. The initial data are taken to be a rest state with superimposed jet localized in the velocity in the $y-$ direction

$$h(x,y,0) = 1.0, \quad u(x,y,0) = 0, \quad v(x,y,0) = 2N_L(x),$$

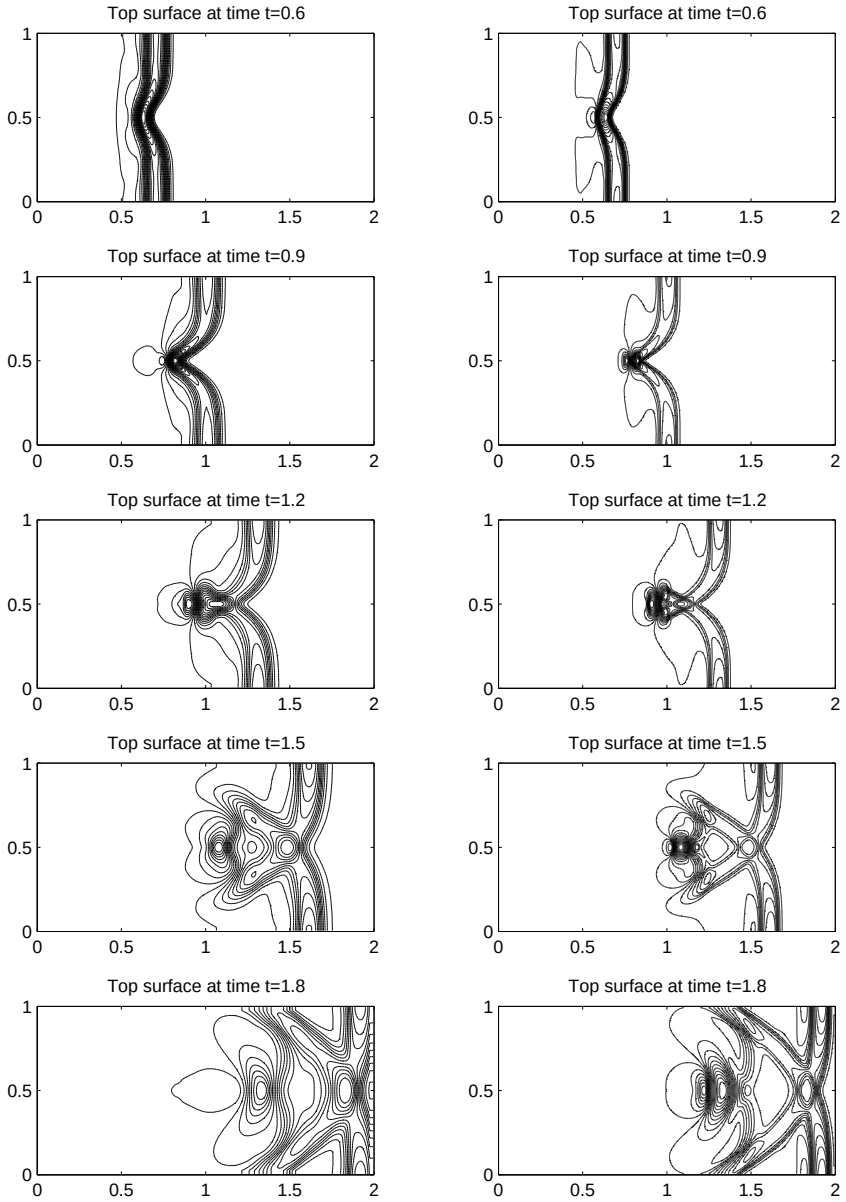

Figure 4: Two dimensional quasi-stationary problem (5.22), (5.23).

where the shape of the velocity v is given by a smooth profile

$$N_L(x) = \frac{(1 + tanh(4x/L + 2))\,(1 - tanh(4x/L - 2))}{(1 + tanh(2))^2}$$

with $L = 2$. We have used flat bottom topography $b(x) = 0$, the parameter of the Coriolis forces f and the gravitational acceleration g are set to 1. The nondimensional parameter representing the effects of Coriolis forces, the Rossby number $Ro = \frac{|v(x,y,0)|}{fL} = 1$ and the Burgers number reflecting the nonlinear effects is $Bu = \frac{g|h(x,y,0)|}{f^2L^2} = 0.25$. The initial jet adjusts a momentum unbalance, which emits the waves, the so-called gravity waves, propagating out from the jet. The formation of shocks can be noticed within the jet core approximately at π/f, which is a half of a natural time scale $T_f = 2\pi/f$, see Figures 5, 6. As time evolves the solution tends to the equilibrium state $fv = gh_x$, which is a geostrophic balance as demonstrated in Figure 7. We can notice that even for long

time simulations there are still small oscillations around the geostrophic equilibrium. As pointed out by Bouchut et al. [5] some wave modes with frequencies close to f remain for a longer time in the core of the jet. Their analysis for a linearized situation shows that they correspond to the gravity wave modes having almost zero group velocity, and thus almost non-propagating. For other extensive study of the stability of jets, which gives interesting eigenfunctions similar to those in Figures 5,6 we refer to [10].

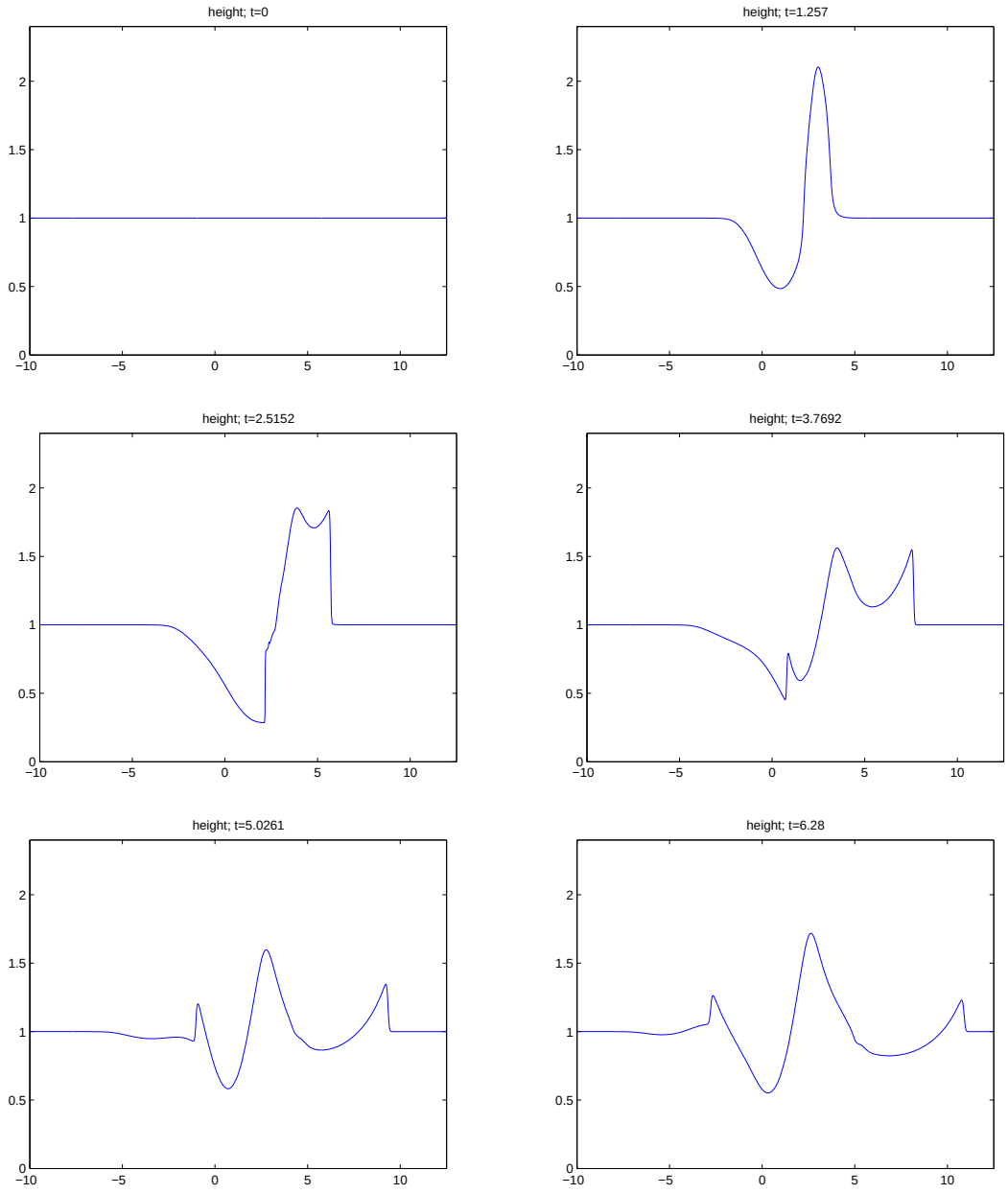

Figure 5: One-dimensional Rossby adjustment problem, time evolution of water height.

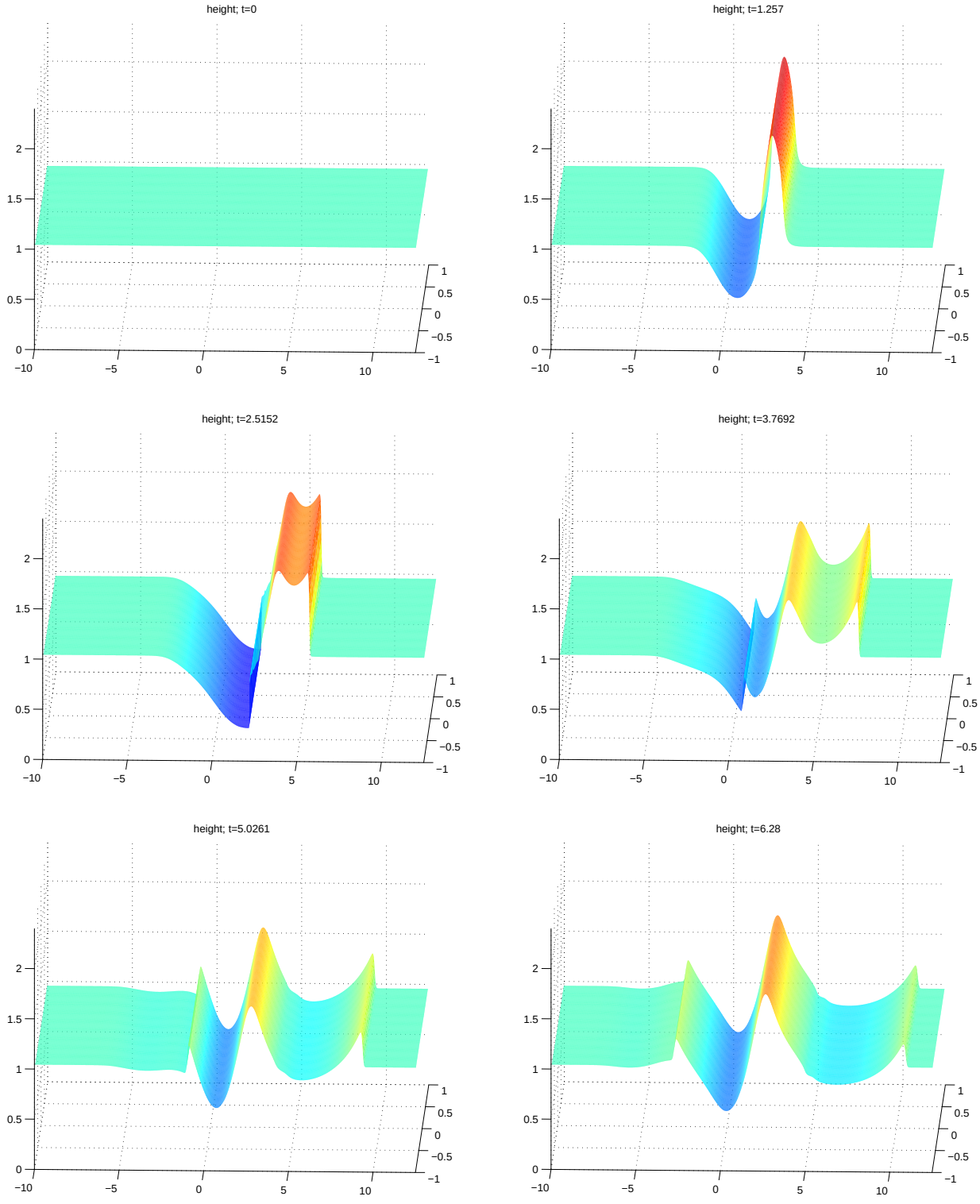

Figure 6: Rossby adjustment problem, time evolution of water height, two-dimensional graphs.

6 Conclusions

In the present paper we have developed a new well-balanced scheme within the framework of the finite volume evolution Galerkin (FVEG) scheme. The scheme is applied for the shallow water equations with source terms modelling the bottom topography and the Coriolis forces. The key ingredient of this FVEG scheme is a new well-balanced version of the multidimensional approximate evolution operator. This approximate evolution operator is used in a predictor step. In fact we are predicting solution at cell interfaces by means of the evolution operator and do not need to use the hydrostatic reconstruction as it is done by Audusse at el. [2].
In the following correction step, which is the finite volume update step, the source term is approximated in the interface-based way. We have proved that the stationary state, the lake at rest situation, and the steady jet in the rotational frame are preserved, cf. Theorem 4.1 and 4.2. Numerical experiments in one- and two-dimensions demonstrate correct resolution of those equilibrium states as well as their small perturbations.
In future we want to extend our study of the well-balanced schemes to the shallow water equations with the source term including moreover nonlinear friction terms, as they appear in oceanographic modelling as well as in the river flow modelling. Another interesting problem arises in the multi-layered shallow water models, which are important in the meteorology and climatology.

Acknowledgements
This research was supported by the Graduate Colleges 'Conservation principles in the modelling and simulation of marine, atmospherical and technical systems' and 'Hierarchy and Symmetry in Mathematical Models' both sponsored by the Deutsche Forschungsgemeinschaft as well as by the EU-Network Hyke HPRN-CT-2002-00282. The authors gratefully acknowledge these supports.

References

[1] Abgrall R, Mezine M. Construction of second order accurate monotone and stable residual distribution schemes for unsteady flow problems. *J. Comput. Phys.* 2003; **188**(1):16-55.

[2] Audusse E, Bouchut F, Bristeau M-O, Klein R, Perthame B. A fast and stable well-balanced scheme with hydrostatic reconstruction for shallow water flows, to appear in *SIAM J. Sci. Comp.* (2004)

[3] Billet S, Toro E.F. On WAF-type schemes for multidimensional hyperbolic conservation laws. *J. Comput. Phys.* 1997; **130**:1-24.

[4] Botta N, Klein R, Langenberg S, Lützenkirchen S. Well balanced finite volume methods for nearly hydrostatic flows. *J. Comp. Phys.* 2004; **196**: 539-565.

[5] Bouchut F, Le Sommer J, Zeitlin V. Frontal geostrophic adjustment and nonlinear-wave phenomena in one dimensional rotating shallow water. Part 2: high-resolution numerical simulations, to appear in *J. Fluid Mech.* 2004.

[6] Csík A, Ricchiuto M., Deconinck H. A conservative formulation of the multidimensional upwind residual distribution schemes for general nonlinear conservation laws. *J. Comput. Phys.* 2002; **179**(1):286-312.

[7] Deconinck H, Roe P, Struijs R. A multidimensional generalization of Roe's flux difference splitter for the Euler equations. *Comput. Fluids* 1993; **22**(2-3):215-222.

[8] Fey M. Multidimensional upwinding, Part II. Decomposition of the Euler equations into advection equations. *J. Comp. Phys.* 1998; **143**:181-199.

[9] Gallouët T, Hérard J-M, Sequin N. Some approximate Godunov schemes to compute shallow-water equations wih topography, *Computers and Fluids* 2003; **32**:479-513.

[10] Gjevik B, Moe H, Ommundsen A. A high resolution tidal model for the area around The Lofoten Islands, northern Norway, *Continental Shelf Research* 2002; **22(1)**: 485-504.

[11] Greenberg JM, LeRoux A-Y. A well-balanced scheme for numerical processing of source terms in hyperbolic equations, *SIAM J. Numer. Anal.* 1996; **33**:1-16.

[12] Klein R. An applied mathematical view of meteorological modelling, *In: Proceedings ICAM 2003*, eds. J.M.Hill and R. Moore, 2003; pp. 227-270.

[13] Kröger T, Lukáčová-Medviďová M. An evolution Galerkin scheme for the shallow water magnetohydrodynamic (SMHD) equations in two space dimensions. *J. Comp. Phys.*, in print 2005.

[14] Kurganov A, Levy D. Central-upwind schemes for the Saint-Venant system. *M^2AN, Math. Model. Numer. Anal.* 2002; **36(3)**:397-425.

[15] LeVeque RJ. Wave propagation algorithms for multi-dimensional hyperbolic systems. *J. Comp. Phys.* 1997; **131**:327-353.

[16] LeVeque RJ. Balancing source terms and flux gradients in high-resolution Godunov methods: The quasi-steady wave propagation algorithm. *J. Comp. Phys.* 1998; **146**:346-365.

[17] Lukáčová-Medviďová M. Multidimensional bicharacteristics finite volume methods for the shallow water equations. In: *Finite Volumes for Complex Applications*, eds. R. Hérbin and D. Kröner, Hermes, 2002, 389-397.

[18] Lukáčová-Medviďová M, Morton KW, Warnecke G. Evolution Galerkin methods for hyperbolic systems in two space dimensions. *MathComp.* 2000; **69**:1355–1384.

[19] Lukáčová-Medviďová M, Morton KW, Warnecke G. On high-resolution finite volume evolution Galerkin schemes for genuinely multidimensional hyperbolic conservation laws, In: *European Congress on Computational Methods in Applied Sciences and Engineering, ECCOMAS 2000*, eds. Onate et al., CIMNE 2000, 1-14.

[20] Lukáčová-Medviďová M, Morton KW, Warnecke G. Finite volume evolution Galerkin methods for Euler equations of gas dynamics. *Int. J. Numer. Meth. Fluids* 2002; **40**(3-4):425-434.

[21] Lukáčová-Medviďová M, Saibertová J, Warnecke G. Finite volume evolution Galerkin methods for nonlinear hyperbolic systems. *J. Comp. Phys.* 2002; **183**:533-562.

[22] Lukáčová-Medviďová M, Morton KW, Warnecke G. Finite volume evolution Galerkin methods for hyperbolic problems. *SIAM J. Sci. Comput.* 2004; **26(1)**:1-30.

[23] Lukáčová-Medviďová M, Warnecke G, Zahaykah Y. On the stability of the evolution Galerkin schemes applied to a two-dimensional wave equation system. submitted, 2004.

[24] Lukáčová-Medviďová M, Warnecke G, Zahaykah Y. Finite volume evolution Galerkin schemes for three-dimensional wave equation system. submitted, 2004.

[25] Noelle S. The MOT-ICE: a new high-resolution wave-propagation algorithm for multi-dimensional systems of conservative laws based on Fey's method of transport. *J. Comput. Phys.* 2000; **164**:283-334.

[26] Noelle S, Pamkratz N, Puppo G, Natvig J. Well-balanced finite volume schemes of arbitrary order of accuracy for shallow water flows. submitted to J. Comput. Phys, 2005.

[27] Shi J. A steady-state capturing method for hyperbolic systems with geometrical source terms. *M^2AN, Math. Model. Numer. Anal.* 2001; **35(4)**:631-646.

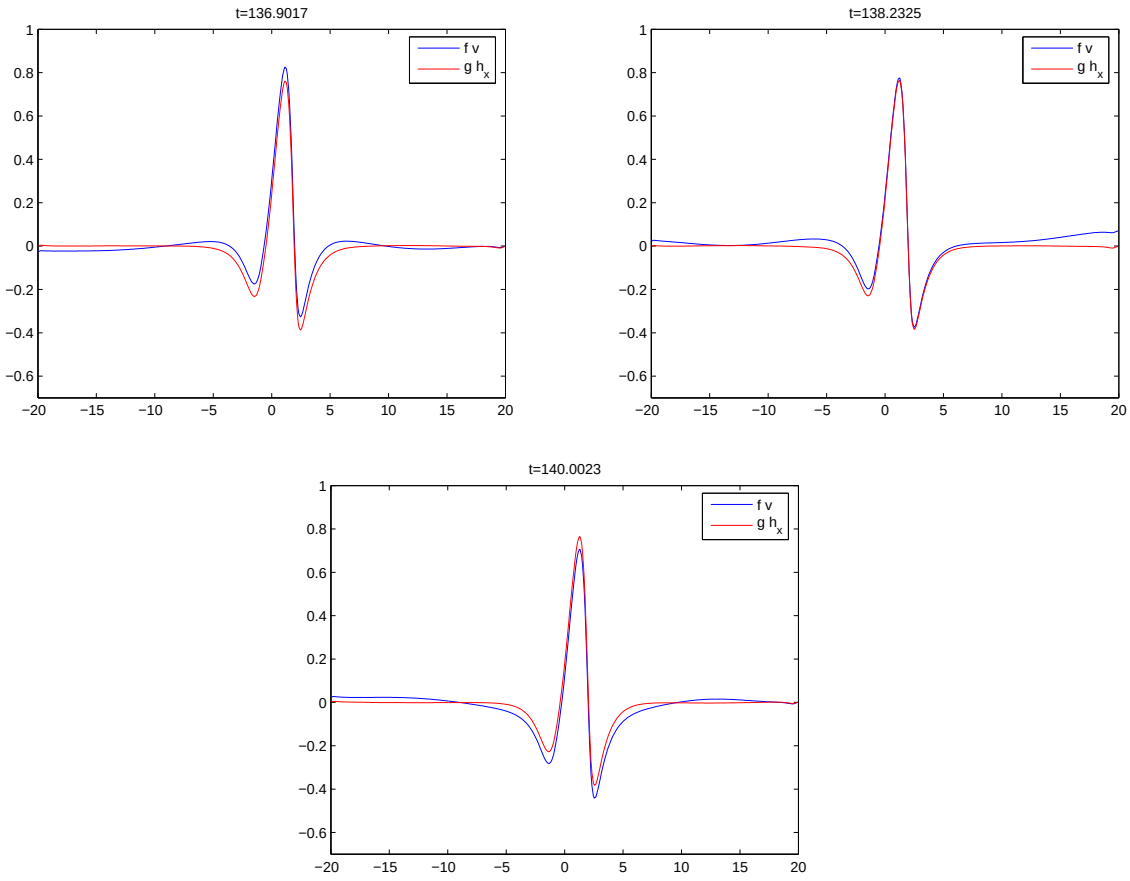

Figure 7: One-dimensional Rossby adjustment problem at different times, geostrophic balance.